Neuroanatomical predictors of real-time fMRI-based emotional brain regulation.

Andrea Caria (andrea.caria@unitn.it)
University of Trento
Alessandro Grecucci
University of Trento

Research Article

Keywords: Emotional brain regulation, anterior insula, real-time fMRI, structural MRI, self-regulation, prediction, kernel ridge regression

Posted Date: April 12th, 2022

DOI: https://doi.org/10.21203/rs.3.rs-1533038/v1

Abstract

Increasing evidence shows that learned control of BOLD activity in selected brain regions can support emotion regulation. Notably, a number of studies demonstrated that regulation of BOLD activity in several emotion-related areas leads to modifications of emotional behavior along with changes of neural activity in local and distributed networks, in both healthy individuals and individuals with emotional disorders. However, to date a comprehensive description of the neural mechanisms underlying self-regulation of the emotional brain is still lacking. Here, we aimed to delineate a neuroanatomical signature predictive of successful real-time fMRI-based anterior insula regulation, a neuromodulation procedure that has been previously shown to elicit changes in emotional stimuli perception in both healthy individuals and patients. Using a kernel ridge regression model, we investigated gray and white matter structural features discriminative of self-regulation of the anterior insula activity. Our multivariate regression analysis revealed that cortical and subcortical regions in the fronto-occipital and medial temporal lobes as well as the basal ganglia and cerebellum were good predictors of self-regulation of the anterior insula. Notably, the cerebellum appeared to have the largest weight for successful prediction of self-regulation of the anterior insula. Overall, our findings revealed a specific neuroanatomical topography relevant to emotional brain regulation. Ultimately, we reason that the observed neuroanatomical predictors of learned regulation might be important for designing and optimizing future protocols of patient-tailored interventions for emotional disorders.

1 Introduction

In the last decade, an increasing number of real-time fMRI studies demonstrated that learned control of localized brain activity is attainable through either explicit or implicit instrumental conditioning paradigms (Caria et al. 2012; Sulzer et al. 2013; Shibata et al. 2019; Paret et al. 2019a; Caria 2016; Lubianiker et al. 2019). Recent development of this approach led to advanced techniques that permit regulation of distributed brain patterns as well of functional connectivity measures (Watanabe et al. 2017; Koush et al. 2017; Ramot et al. 2017; Morgenroth et al. 2020). Increasing evidences show that learned control of BOLD activity in selected brain regions can support emotion regulation (Linhartova et al. 2019; Shibata et al. 2016; Paret and Hendler 2020). In fact, several investigations demonstrated that emotion regulation can be mediated by voluntary regulation of key emotional brain centers such as the amygdala (Zotev et al. 2011; Hellrung et al. 2018; Paret et al. 2016b; Paret et al. 2018; Marxen et al. 2016; Bruhl et al. 2014; Herwig et al. 2019; Paret et al. 2014), anterior insula (AI) (Berman et al. 2013; Caria et al. 2010; Caria et al. 2007; Lawrence et al. 2013; Cohen Kadosh et al. 2016; Yao et al. 2016; Zilverstand et al. 2015; Veit et al. 2012) and anterior cingulate cortex (Grone et al. 2015; Hamilton et al. 2011). Remarkably, a number of studies showed that regulation of BOLD activity in these areas leads to modifications of emotional behavior along with changes of neural activity in local and distributed networks, in both healthy (Caria et al. 2010; Yao et al. 2016; Zilverstand et al. 2015; Koush et al. 2017) and diseased conditions such as depression (Mehler et al. 2018; Young et al. 2017a; Young et al. 2017b; Young et al. 2018b; Young et al. 2018a; Zotev et al. 2016; Yuan et al. 2014), anxiety disorders (Scheinost et al. 2013; Zilverstand et al. 2015; Morgenroth et al. 2020) and posttraumatic stress disorder (Misaki et al. 2018; Zotev et al. 2018; Zweerings et al. 2018). Altogether these findings proved real-time fMRI-neurofeedback a promising neuromodulatory technique for developing novel treatments of emotional disorders (Paret and Hendler 2020).

However, several neuropsychological and methodological aspects still remain unclear and sometimes controversial (Paret et al. 2019a; Thibault et al. 2018). For instance, although some hypotheses and empirical indications of the neural mechanisms leading to changes at neural and behavioral level were recently proposed (Sitaram et al. 2017; Shibata et al. 2019; Gaume et al. 2016; Emmert et al. 2016), a comprehensive description is still lacking. A previous meta-analysis of studies focusing on regulation of several different brain area identified a possible “regulation network” including the lateral prefrontal cortex, anterior insula, basal ganglia, temporo-parietal areas, anterior cingulate and visual associative areas (Emmert et al. 2016). However, most of the studies included in this meta-analysis have targeted areas that were directly or indirectly involved in emotional behavior, making then difficult to conclude on the general role of the identified regions. Additional studies in the specific context of emotional brain regulation corroborated and extended these evidences by showing a differential involvement of prefrontal and orbitofrontal cortices and striatum in relation to feedback control, monitoring and reward (Paret et al. 2019b; Paret et al. 2018; Paret et al. 2016a; Paret et al. 2016b). Basal ganglia, in particular the striatum, would mediate instrumental and reinforcement learning independently of functional domain (Skottnik et al. 2019; Shibata et al. 2019). Similarly, the role of frontoparietal, anterior insula, anterior cingulate cortex, regions typically involved in several different cognitive functions, appears to support general real-time fMRI-based regulation (Shibata et al. 2019) and BCI control (Papageorgiou et al. 2013). A recent investigation aimed to identify predictors of successful self-regulation on the basis of a cohort of heterogenous pretraining functional data from studies targeting several different areas in both healthy participants and patients (Haugg et al. 2020). In this study, no common brain-based success predictors emerged, possibly because of differential functional mechanisms influencing learned brain regulation within distinct functional domains. On the other hand, Zhao and colleagues exploring possible associations between brain structure and real-time fMRI neurofeedback learning showed that the gray matter (GM) volume of the right putamen could significantly predict learning success across the three different data sets implying distinct experimental designs and the targeted training regions (Zhao et al. 2021). This evidence

confirmed previous indications pointing to the striatum, and its well-recognized role in instrumental and associative learning, as key node for real-time based brain regulation (Sitaram et al. 2017). In their analysis, Zhao and colleagues included previous real-time fMRI studies targeting the anterior insula, amygdala and anterior cingulate cortex, which are all regions relevant to emotional behavior, however, no additional regions implicated in general emotion regulation emerged (Etkin et al. 2015; Grecucci et al. 2013a; Grecucci et al. 2013b; Messina et al. 2021). On the other hand, we previously showed that self-regulation of AI is functionally mediated by regions in the cortical emotion regulatory network (Etkin et al. 2015), and also relies on more archaic core emotional and motivational centers in the upper mesencephalon (Caria 2020). Moreover, these results corroborated indications of possible similarities between circuits associated with cognitive emotion regulation and those involved in self-regulation of emotional brain regions (Etkin et al. 2015; Emmert et al. 2016; Paret and Hendler 2020; Caria 2020; Gross 2014).

Until know, neuroanatomical and neurofunctional substrate specifically supporting real-time fMRI-based emotional brain regulation still remain unclear. Here, in an attempt to delineate a neuroanatomical signature of real-time fMRI-based emotional brain regulation, we used a kernel ridge regression model (Kong et al. 2019) to assess whether individual volumetric variability of gray and white matter (GM, WM) influences self-regulation of AI (Caria et al. 2010; Caria et al. 2007).

Real-time fMRI-based learned regulation of AI activity has been proved to be an effective neuromodulation procedure eliciting changes in emotional stimuli perception in both healthy individuals and patients with emotional disorders (Caria et al. 2010; Caria et al. 2007; Ruiz et al. 2013; Sitaram et al. 2014; Yao et al. 2016; Linden et al. 2012; Zilverstand et al. 2015).

We then also estimated predictability of AI regulation on the basis of selected well-known GM networks. In line with previous functional studies indicating a main involvement of regions in the central executive network (CEN) and salience network (SN) during both real-time fMRI-based regulation and emotion regulation (Caria 2020; Buhle et al. 2014; Etkin et al. 2015; Kohn et al. 2014; Ochsner et al. 2012; Emmert et al. 2016), we expected that structural characteristics of some of these regions, such as prefrontal circuits and basal ganglia, might significantly contribute to predict successful AI regulation.

2 Materials And Methods

Our data set was composed of data from two previous studies demonstrating successful real-time fMRI-based regulation of the BOLD signal in AI (Caria et al. 2007; Caria et al. 2010). Both studies were approved by the local ethics committee of the University of Tübingen, Germany and all participants signed informed consent.

Participants

Eighteen right-handed participants from the two above-mentioned studies (9 women; mean age = 24.64, SD = 4.40) were included. Participants from previous control groups were unfortunately not included because of unequal and lower sample size. All participants had no history of neurological or psychiatric disorders including substance abuse/dependence and psychotropic medications.

MRI data acquisition

All functional images were acquired using a 3.0 T MR Siemens scanner, with a 12 channels head coil (Siemens Magnetom Trio Tim, Siemens, Erlangen, Germany). During real-time fMRI-based emotion regulation, standard echo planar imaging (EPI) images consisting of sixteen axially oriented slices (voxel size = 3×3×5 mm^3, slice gap = 1 mm) were acquired (repetition time TR = 1500 ms, matrix size = 64×64, FoV = 192x192mm, TE = 30 ms). Considering that the primary respiratory-related component of the fMRI signal usually fluctuates at about 0.3 Hz, a TR equal to 1.5s prevents aliasing of the first respiratory harmonics with spectral signature of the typical BOLD effect (Caballero-Gaudes and Reynolds 2017). Additionally, a gradient echo field map (TR 488 ms, TE 1 = 4.49 ms, TE 2 = 6.95 ms) and a T1-weighted MPRAGE structural scan (matrix size = 256 x 256, 160 partitions, 1 mm^3 isotropic voxels, TR = 2300 ms, TE = 3.93 ms, TI = 1100 ms, $\alpha = 8°$) were acquired from each participant to reduce geometric distortion due to magnetic field inhomogeneities (Togo et al. 2017). In order to minimize head movements two foam cushions were positioned around participant's head.

Real-time fMRI paradigm

The real-time fMRI paradigm consisted of emotion regulation runs guided by online feedback of fMRI signal in the AI. Participants were provided with online continuous feedback through a visual display consisting of a graduated thermometer depicting changes of BOLD response with increasing or decreasing number of bars updated every 1.5s. Four emotion regulation runs composed of several blocks (16 blocks for n = 9; 20 blocks for n = 9) were performed in one day. Each run consisted of *up regulation* blocks (22.5s n = 9; 30s n = 9), cued with an arrow at the right side of the thermometer, alternating with *down regulation* blocks (22.5s n = 9; 30s n = 9), cued with a cross hair at

the right side of the thermometer. Participants were instructed that during *up and down regulation* blocks they had to attempt to modulate the intensity of recalled emotional memories and imagery of personally relevant affective episodes guided by increasing or decreasing number of thermometer bars. The feedback represented the averaged BOLD signal in the AI normalized with respect to a reference region, calculated during *up regulation* with respect to *down regulation*. Three consecutive TRs were considered to reduce rapid signal fluctuations; the first ten volumes of each session were excluded to account for T1 equilibration effects. The target right AI (n = 9, from (Caria et al. 2007)) was selected anatomically based on the high resolution T1 structural scan and consisted of a rectangular area of 4 x 5 voxels on a single slice. The target left AI (n = 9, from (Caria et al. 2010)) was selected anatomically and functionally, through a localizer session consisting of five alternating emotional recall and baseline blocks, and consisted of a rectangular area of 5 x 5 voxels on a single slice. In both studies a similar reference region of interest consisting in large background area not encompassing emotion related areas was used to cancel out global effects and unspecific activations. Participants were informed that the feedback information was delayed of about 1.5s due to online data analysis in addition to a physiological latency of the hemodynamic response of about 6s. Participants were instructed not to move during all the experimental conditions, and informed that physiological signals were monitored. During real-time fMRI training functional images were exported online from the MR console computer to a separate computer for real-time preprocessing and analysis with Turbo brain voyager (Brain Innovation, Maastricht, The Netherlands). Online preprocessing included incremental 3D motion correction and drift correction. Incremental statistical data analysis was based on recursive least squares General Linear Model (GLM).

Offline fMRI data analysis

fMRI data preprocessing and analysis were performed using SPM12 (Wellcome Trust Centre for Neuroimaging, London, UK) and Matlab (The MathWorks, Inc., Natick, MA, US). For each participant, all functional images were first realigned to the mean image using least squares and a 6 parameter (translations and rotations in space) and including resampling using 2nd degree B-spline interpolation, then unwarped and corrected for geometric distortions using the fieldmap of each participant. The high-resolution T1 image was co-registered to the mean image of the EPI series using a rigid body model, estimated with mutual information. Segmentation parameters were used to normalize the functional images to the Montreal Neurological Institute (MNI) space. Last, normalized images were spatially smoothed with a 6 mm FWHM Gaussian kernel in order to balance effect size, spatial accuracy and statistical significance estimated using Gaussian random fields (Worsley and Friston 1995; Stelzer et al. 2014).

A fixed-effects general linear model (GLM) was used to perform first-level statistical analysis. Hemodynamic response amplitudes were estimated using standard regressors, constructed by convolving a boxcar function, for up and down emotion regulation, with a canonical hemodynamic response function using standard SPM12 parameters. The time series in each voxel were high-pass filtered at 1/128s to remove low frequency drifts. An autoregressive AR(1) model was employed to address autocorrelation in the timeseries. Contrast images of up emotion regulation versus down emotion regulation were created for each block and run. Movement parameters were also included into the GLM as covariates to account for head motion artifacts. Second level random effects group analysis was performed by entering single subject contrast images into one sample t-tests. Whole brain statistical maps were thresholded at $p < 0.001$ corrected at cluster level for multiple comparison using probabilistic threshold-free cluster enhancement (pTFCE) (Smith et al. 2009; Spisak et al. 2018), an approach that integrates cluster information into voxel-wise statistical inference so as to enhance detectability of neuroimaging signal and to control for Type I error. Estimation of BOLD signal changes in the AI during real-time fMRI training was performed using regions-of-interest (ROIs) analysis (Poldrack 2007; Cremers et al. 2017) in the targeted ROIs (see further details in (Caria et al. 2007; Caria et al. 2010)). AI regulation during real-time fMRI training was assessed by testing single subject's BOLD signal change across runs for the contrast up > down emotion regulation using bootstrap analysis (1000 bootstrap samples, 95% bias corrected and accelerated confidence interval), as implemented in SPSS statistics software (v.24, IBM Corp. Armonk, NY).

Data from run 4 were not included as not every participant underwent all four runs (14 out of 18).

In addition, as indication of successful real-time fMRI-based regulation we considered the BOLD amplitude difference between last and first run and an index of learning, calculated as the slope of the linear curve that fitted % BOLD amplitudes during each run. These learning-related values, along with the averaged BOLD activity of all runs, were then used in the subsequent multivariate pattern regression analysis. The averaged activity was manly expected to be representative of the whole self-regulation session but possibly also reflecting non-linear learning.

Anatomical-based pattern regression analysis

Structural MR data were used in a regression-based multivariate pattern analysis (MVPA), as implemented in PRoNTo toolbox (version 2.1, http://www.mlnl.cs.ucl.ac.uk/ pronto, (Schrouff et al. 2013), to investigate structural patterns of white and gray matter predictive of real-

time fMRI-based AI regulation. Quality check of the initial images was first performed to exclude evident artefacts. The anatomical scan of one participant had to be excluded because of poor image quality. Images were segmented into gray matter (GM) and white matter (WM) partitions using the segmentation procedure (Ashburner and Friston 2005) as implemented in SPM12 (Statistical Parametric Mapping software, version 12; http://www.fil.ion.ucl.ac.uk/spm; Wellcome Department of Imaging Neuroscience, London), normalized to MNI space and spatially smoothed (full-width at half maximum of Gaussian smoothing kernel [8, 8, 8]). Multivariate regression analysis was performed using Kernel ridge regression (KRR). KRR is a multivariate regression method equivalent to maximum a posteriori approach to Gaussian process regression with fixed prior variance and no explicit noise term. KRR is the dual-form formulation of ridge regression that enable to solve regression problems with high dimensional data in a computationally efficient way. Linear kernels were built separately for each feature sets: whole brain smoothed GM and WM volume images. Age and gender were regressed out. The predictive function was defined during a training phase where patterns from input were analyzed in order to predict BOLD values changes over training runs (excluding Run 4). Hyperparameters were optimized as suggested by PRONTO developers with soft-margin C ranging from 0.0001, 0.01, 1, 10, 100, 1000, to compute the inner loop and the outer loop (model performance). Cross validation was based on a leave-one-subject-out (LOSO) framework: for each fold, one input image was left out and served as the testing set. The kernel ridge regression model was trained to associate percentage of BOLD change in the AI with the multivariate information in our sample of participants (Yang et al., 2016). The trained kernel ridge regression model was then used to predict BOLD change in the left-out image. This step was repeated for each of the 17 folds. Across all folds, predictive accuracy was calculated as the Pearson's correlation coefficient (r), coefficient of determination (R2), and normalized mean squared error (nMSE) between predicted and actual real-time fMRI training effectiveness (Yang et al. 2016). Statistical significance of the classifications was estimated using 5000 permutations with random assignment of group class to input image. For each iteration, the regression targets were randomly permuted across all participants and cross-validation procedure was repeated. Gray matter regions were identified according to the Automated Anatomical Labeling (AAL) atlas (available on the WFU-PickUp Atlas toolbox of SPM12 (Tzourio-Mazoyer et al. 2002), a manual macroanatomical parcellation of single subject MNI-template brain consisting of 116 brain regions and additionally including brainstem regions. We also estimated predictability of AI regulation on the basis of well recognized networks such as the default-mode network (DMN), central executive network (CEN), salience network (SAL), visual network (VIS) and sensorimotor network (SMN) (Damoiseaux et al. 2006; Smith et al. 2009; Doucet et al. 2019). The ICBM DTI-81 Furthermore, white matter regions predictive of AI regulation were assessed on the basis of the stereotaxic probabilistic white matter atlas, that fuses DTI-based white matter information with the anatomical template ICBM-152 (Mori et al. 2008; Hua et al. 2008). Finally, the weight maps for the KRR model showing statistically significant values of correlation and normalized MSE were obtained. The weight map spatially represents the model's weights in % by showing the contribution of each voxel in the image (Schrouff et al. 2018; Schrouff et al. 2013). The weight map of linear machine learning models is the average map across the cross-validation folds divided by its Euclidean norm (Schrouff et al. 2013). In addition, the normalized weight for each brain structure is calculated as the average of absolute values of all voxel weights within each region defined by the AAL divided by the number of voxels within the region. Labelled regions were then ranked according to the percentage of the total normalized weights they explained.

3 Results

Self-regulation of AI activity

As reported in our previous studies (Caria et al. 2010; Caria et al. 2007), most of participants in the two groups achieved successful regulation of AI activity during real-time fMRI training as evidenced by significant differences between first and last run in each group separately. This effect was confirmed when both groups were merged together as shown by repeated measures ANOVA ($F_2 = 3.63$ $p = 0.38$, with a significant linear trend $F_1 = 5.02$ $p = 0.40$) (Fig. 1) and post hoc analysis revealing a significant difference between first and last run (run3) (paired-samples t test, $t_{17} = 2.24$ $p = 0.04$) and between first and second run ($t_{17} = 2.34$ $p = 0.03$). As previously reported, successful regulation was attained through a combination of real-time fMRI feedback and emotion-related mental strategies, and differed from the effects observed in two control groups tested with either unspecific real-time fMRI feedback or mental imagery alone(see (Caria et al. 2010; Caria et al. 2007) for more complete information).

Pattern regression analysis

Whole brain KRR-based multivariate pattern analysis permitted to identify gray matter and white matter regions predictive of individual differences in self-regulation of AI activity during real-time fMRI-based emotion regulation.

GM whole brain results

The GM network predictive of Run1 is reported in Table 1 (r = 0.39 p = 0.051, R2 = 0.15 p = 0.257 nMSE = 0.10 p = 0.055). This network consisted of extended areas mainly in the frontal, prefrontal and occipital cortices, cerebellum as well as globus pallidus and caudate nucleus. No significant results were observed for Run2 (r = -0.16 p = 0.544, R2 = 0.02 p = 0.693 nMSE = 0.22 p = 0.841). Brain regions predictive of Run3 are also reported in Table 1 (r = 0.47 p = 0.028, R2 = 0.22 p = 0.257 nMSE = 0.07 p = 0.025). In this condition, a less distributed anatomical network with respect to Run1, mainly involving the cerebellum and medial temporal regions and including dorsomedial and dorsolateral prefrontal cortex is observed. Table 1 and Fig. 2 report GM regions that successfully predicted averaged AI activity of all runs (r = 0.49 p = 0.049, R2 = 0.24 p = 0.168 nMSE = 0.07 p = 0.049). These results revealed a large network including portions of the cerebellum, frontal and prefrontal cortex including dorsomedial and dorsolateral areas, the right inferior and superior temporal gyrus and supramarginal gyrus, the occital cortex, hipoccampus and parahippocampal gyrus, and the globus pallidus. No significant results emerged when either the index of learning or the difference between the last and first run were considered.

Table 1

All Runs			Run1			Run3		
GM regions	Weight (%)	Voxels	Area	Weight (%)	Voxels	Area	Weight (%)	Voxels
Cerebellum_10_R	1,52	286	Vermis_10	1,6468	264	Cerebellum_10_R	2,2455	286
Frontal_Sup_Medial_R	1,4755	4426	Cerebellum_9_R	1,6184	1320	Temporal_Pole_Sup_R	1,8242	2085
Frontal_Sup_Orb_R	1,4696	1352	Frontal_Mid_Orb_L	1,5927	2061	Cerebellum_7b_R	1,7045	692
Temporal_Pole_Sup_R	1,4676	2085	Calcarine_L	1,563	5182	Temporal_Pole_Mid_R	1,6092	1810
Frontal_Mid_Orb_R	1,4606	1769	Frontal_Inf_Orb_R	1,4951	3635	Temporal_Pole_Sup_L	1,5656	2708
Frontal_Sup_L	1,3404	8157	Frontal_Sup_Medial_R	1,4859	4426	Frontal_Inf_Tri_R	1,3968	3654
Temporal_Inf_R	1,3332	7209	Frontal_Sup_Medial_L	1,4179	6643	Cerebellum_Crus2_R	1,3955	3901
Fusiform_R	1,3274	5731	Frontal_Mid_Orb_R	1,3643	1769	Cerebellum_8_L	1,3869	2619
Frontal_Inf_Orb_R	1,327	3635	Frontal_Inf_Orb_L	1,3306	4083	Temporal_Inf_R	1,38	7209
Cerebellum_9_L	1,3235	1407	Occipital_Inf_L	1,2929	2264	Cerebellum_8_R	1,3715	2603
Cerebellum_7b_R	1,3198	692	Frontal_Sup_Orb_R	1,2566	1352	Cerebellum_9_L	1,331	1407
Frontal_Sup_Medial_L	1,2971	6643	Cerebellum_9_L	1,2385	1407	Cerebellum_9_R	1,3218	1320
Cerebellum_8_L	1,2659	2619	Occipital_Inf_R	1,2259	2411	Temporal_Inf_L	1,308	7081
Cerebellum_8_R	1,2448	2603	Temporal_Pole_Mid_R	1,203	1810	Occipital_Inf_L	1,2411	2264
Cerebellum_Crus1_R	1,2121	4791	Cerebellum_7b_R	1,1814	692	Frontal_Mid_Orb_R	1,2325	1769
Pallidum_L	1,2088	637	Vermis_9	1,1731	388	Frontal_Mid_R	1,212	9213
Frontal_Mid_Orb_L	1,1921	2061	Frontal_Sup_Orb_L	1,1658	1666	Fusiform_R	1,206	5731
Rectus_L	1,1774	1780	Temporal_Inf_L	1,1611	7081	Cerebellum_Crus1_R	1,2016	4791
Frontal_Mid_R	1,1595	9213	Cerebellum_Crus1_L	1,151	5334	Frontal_Inf_Oper_R	1,1978	2838
Frontal_Sup_Orb_L	1,1351	1666	Temporal_Inf_R	1,1464	7209	Calcarine_R	1,1702	4235
Frontal_Sup_R	1,1123	8047	Occipital_Mid_L	1,1425	7552			
Frontal_Mid_L	1,0963	11129	Lingual_L	1,1325	5201			
Cerebellum_Crus2_R	1,0879	3901	Pallidum_L	1,1213	637			
ParaHippocampal_R	1,0774	2557	Heschl_R	1,0985	513			
SupraMarginal_R	1,0714	3768	Caudate_L	1,098	2212			
Hippocampus_R	1,0659	2296	Frontal_Mid_L	1,0879	11129			
Occipital_Inf_L	1,0611	2264	Cingulum_Mid_L	1,0713	4478			
Calcarine_R	1,0574	4235	Frontal_Sup_L	1,058	8157			
Cerebellum_Crus1_L	1,0452	5334	Pallidum_R	1,0342	608			
Temporal_Pole_Sup_L	1,0173	2708	Lingual_R	1,0032	5574			
			Frontal_Inf_Oper_R	1,0032	2838			

GM network-based results

Multivariate regression analysis based on selected brain networks showed a larger predictive effect of VIS, CEN and DMN (r = 0.41 p = 0.038, R2 = 0.17 p = 0.298 nMSE = 0.10 p = 0.047) for Run1 (see Table 2). No significant effects were measured for Run2 and Run3. A major contribution of DMN and CEN in predicting average AI activity across runs (% weight DMN: 22.86, CEN: 21.97, SMN: 18.93, SAL: 18.52, VIS: 17.72, r = 0.43 p = 0.043, R2 = 0.19 p = 0.292 nMSE = 0.08 p = 0.046; see Table 2). No significant results emerged when either the index of learning or the difference between the last and first run were considered.

Table 2

All Runs			Run1			Run3		
Network	Weight (%)	Voxels	Network	Weight (%)	Voxels	Network	Weight (%)	Voxels
DMN	22,86	23635	VIS	22,96	21163	CEN	21,68	16778
CEN	21,97	16778	CEN	21,39	16678	VIS	20,79	21163
SMN	18,93	20757	DMN	21,27	23635	SMN	20,59	20757
SAL	18,52	9753	SAL	17,92	9753	DMN	18,51	23635
VIS	17,72	21163	SMN	16,44	20757	SAL	18,4	9753

WM results

No significant results were observed when each run was considered separately. However, Table 3 and Fig. 3 report white matter regions that successfully predicted averaged AI activity across all runs (r = 0.49 p = 0.034, R2 = 0.24 p = 0.170 nMSE = 0.07 p = 0.033). The tapetum, fronto-occipital fasciculus, fornix and posterior thalamic radiation were among the regions showing the highest predictive value as indicated by the normalized weight. No significant results again emerged when either the index of learning or the difference between the last and first run were considered.

Table 3

WM regions	Side	Weight (%)	Voxels
Tapetum	L	5,52	171
Inferior fronto-occipital fasciculus	L	5,42	554
Fornix /Stria terminalis	L	4,32	329
Posterior thalamic radiation	L	3,85	1182
Uncinate fasciculus	L	3,68	171
Posterior corona radiata	L	3,53	1074
Uncinate fasciculus	L	3,42	544
Cingulum (hippocampus)	R	3,29	844
Superior corona radiata	R	3,26	2057
Superior longitudinal fasciculus	R	3,23	331
Cingulum (cingulate gyrus)	L	3,10	703
Superior fronto-occipital fasciculus	R	3,08	1930
Sagittal stratum	R	3,04	1209
External capsule	L	3,04	1059
Sagittal stratum	L	3,03	624
Posterior corona radiata	R	3,01	2158
Fornix		2,90	3684
Posterior limb of internal capsule	R	2,56	917
Cingulum (cingulate gyrus)	R	2,55	1057
Cingulum (hippocampus)	L	2,46	287
Anterior corona radiata	L	2,39	2057
Middle cerebellar peduncle		2,32	477476
Inferior fronto-occipital fasciculus	R	2,29	122
Posterior corona radiata	L	2,23	1087
Retrolenticular part of internal capsule	R	2,21	1166
Superior longitudinal fasciculus	L	2,17	1930
Splenium of corpus callosum	L	2,14	4214
Body of corpus callosum		1,96	2583
External capsule	R	1,61	636
Tapetum	L	1,55	87
Superior corona radiata	L	1,51	2150
Posterior limb of internal capsule	L	1,36	1166
Fornix (cres) / Stria terminalis	R	1,24	234
Retrolenticular part of internal capsule	L	1,24	763
Anterior limb of internal capsule	L	1,13	960
Uncinate fasciculus	L	1,10	65

4 Discussion

The main objective of this study was to identify a possible neuroanatomical signature of real-time fMRI-based emotional brain regulation by detecting structural features predictive of AI-guided emotion regulation. To this aim, we used a KRR model to estimate the predictive value of GM and WM regional volume for individual differences in self-regulation of AI activity. Our multivariate regression analysis revealed that both GM and WM volumetric characteristics of several cortical and subcortical areas successfully predicted regulation of AI activity, considering either single runs or averaged activity of all runs. Overall, the individual predictive value of both GM and WM regions was rather small suggesting that successful prediction mainly relied on a combined effect of specific anatomical networks. Accordingly, GM network-based analysis indicated significant predictive values, in particular of the DMN and CEN, and to a lesser extent of the SN.

Altogether, these findings represent an indication that volumetric differences of specific neuroanatomical structures can impact the ability to attain voluntary regulation of emotional brain activity. However, the nature of neuroanatomical differences affecting self-regulation of brain activity is likely heterogenous and cannot be simplistically considered unidirectional. As multivariate regression analysis is sensitive to any systematic volumetric difference contributing to prediction of behavioral data, independently of directionality, our results should be interpreted as the effect of both increased and reduced GM and WM volumetric characteristics that altogether influence AI regulation performance.

Nevertheless, our results revealed that several GM regions including areas in the prefrontal cortex, medial temporal cortex, lateral occipital cortex, globus pallidus, hippocampus, parahippocampal gyrus and the cerebellum, as well as WM regions including the fronto-occipital fasciculus, tapetum and fornix, were successful predictors of overall self-regulation of AI activity.

We have not observed any GM and WM region predictive of learning-related indices. This result might be related to the heterogeneity of learning strategies among participants as well as to non-linear learning curves across runs. On the other hand, average AI activity might partially capture individual differences and more complex learning processes associated to emotional brain regulation.

In addition, analysis of single runs appears to reflect well-known learning effects. For instance, in accordance with previous functional studies (Lee et al. 2011) our results showed that the predictive anatomical network is more circumscribed in the last run, a phase when regulation is usually more consolidated, whereas in the initial phase the structural pattern is more distributed. Notably, common frontal, prefrontal, occipital, medio-temporal and cerebellar regions are observable in both first and last run, whereas the caudate and pallidum contribute only to the first run. Moreover, the cerebellum, although it participates to prediction of AI activity during both first and last run, has the largest weight in the last run when participants attained the highest increase of AI activity.

Our findings are generally in line with previous real-time fMRI studies as well as recent theoretical models on the general neural mechanisms underlying brain regulation, both indicating increased activity of the dorsolateral prefrontal cortex and lateral occipital cortex associated with attentional processes in relation to feedback control (Paret et al. 2018; Sitaram et al. 2017; Shibata et al. 2019; Caria 2020), and also pointing to the basal ganglia as critical regions for core learning-related processes such as salience-based strategy selection and reinforcement assessment (Skottnik et al. 2019). In our analysis, the striatum contributes only to the first run and not to the last, it is then conceivable that the observed attenuation might be related to a decreased relevance of strategies' individuation process when regulation is more easily attainable.

The ventral striatum has been also proposed to enable monitoring the implicit reward value of fMRI feedback (Paret et al. 2018; Sitaram et al. 2017), whereas the orbitofrontal cortex would process feedback failure-associated signals (Paret et al. 2019b). In addition, other regions such as the insula and anterior cingulate cortex (Emmert et al. 2016; Paret et al. 2019a; Shibata et al. 2019) would participate to regulation processes, likely by supporting continuous error monitoring and evaluation (Gaume et al. 2016). Our results, unlike these previous evidences, suggest that structural differences of the SAL network, including anterior cingulate gyrus, amygdala, ventral striatum and SN/VTA, might be less relevant for predicting AI regulation.

On the other hand, in line with previous functional data (Shibata et al. 2019), we observed a remarkable influence of cerebellar structures for learned regulation. The cerebellum, besides its clear role in adaptive motor learning (Galea et al. 2011), is implicated in higher-level cognitive functions such as encoding of internal models of mental representations (Ito 2008; Sokolov et al. 2017). It also contributes to adaptive predictive mechanisms during error-based and reinforcement learning (Swain et al. 2011; Ito 2008; Sokolov et al. 2017). An increasing number of studies demonstrated that the cerebellum processes reward- and error-related signals (Heffley and Hull 2019; Kostadinov et al. 2019; Larry et al. 2019; Sendhilnathan et al. 2020; Wagner et al. 2017). Existing interconnections of the posterior cerebellum with ventral and dorsal striatum (Bostan et al. 2013) might then support exchanging of reward- and error-related information during real-time fMRI training. The cerebellum has been recently described as part of an integrated network along with basal ganglia, and

prefrontal cortex subserving multiple non-motor functional domains (Bostan and Strick 2018) including affective and socio-cognitive behavior (Sokolov et al. 2017; Van Overwalle et al. 2014; Pierce and Peron 2020). The widespread cerebellar interplay with several regions of the limbic network might then support a modulatory function during emotion regulation (Baumann and Mattingley 2012; Schutter and van Honk 2009; Pierce and Peron 2020). Cerebellum-mediated adaptive predictive mechanisms would enable selection and adjustment of appropriate regulatory strategies. During our real-time fMRI training participants explicitly induced self-generated affective states through emotional recalling and autobiographical memory retrieval. The efficacy of different emotional strategies was then continuously estimated and assessed so as to retain and fine-tune those more predictive of successful regulation. A probabilistic representation of the adopted emotional strategies was thus likely implemented and dynamically updated. Additional networks such as the DMN, might also support the instantiation of predictable future events (Suddendorf and Corballis 2007; Spreng and Grady 2010). The DMN is posited to constitute a reinforcement learning agent mediating higher order predictive control of behavior through decision process based on prediction error estimation and reward feedback assessment (Dohmatob et al. 2020). In line with this perspective, the DMN along with the CEN might thus play an important role in real-time fMRI-mediated regulation of brain activity.

Emotional imagery and affective memory recalling have been proved effective in supporting emotional brain regulation (Linhartova et al. 2019). Interindividual differences in the capacity to adopt such strategies, possibly reflected by specific neuroanatomical features, are then expected to significantly influence brain regulation ability. Accordingly, our results showed that volumetric differences of medial temporal regions such as the perirhinal cortex, hippocampus and parahippocampal gyrus, as well as the fornix, all regions implicated in autobiographical memory and emotional memory retrieval (Ritchey et al. 2019; LaBar and Cabeza 2006), were good predictors of AI regulation. Overt self-regulation might then capitalize on the capacity to adopt explicit emotional strategies that rely on structural and functional characteristics of the medial temporal lobe. On the other hand, a number of studies demonstrated that brain activity can be actually regulated implicitly, without specific instructions, and even covertly with participants being not aware of the regulation process (Ramot et al. 2016; Watanabe et al. 2017; Taschereau-Dumouchel et al. 2018).

Finally, our results are also in line with studies investigating the neural correlates of cognitive emotion regulation (Gross 2014). For instance, we also observed involvement of the dorsolateral and medial prefrontal cortex regions, assumed to mediate top-down emotional regulatory processes. However, these regions were typically associated with down-regulation of emotions, whereas in our study participants were mainly instructed to up-regulate AI activity. Disentangling the specific impact of these regions on both regulation conditions separately it was here not possible as up-regulation activity was strictly dependent on the following down-regulation phase, not having a baseline condition. In future studies, it would be interesting to investigate whether morphological characteristics of the frontal and prefrontal circuits differentially affect up and down emotional brain regulation.

In conclusion, our findings corroborate previous functional evidences of brain networks implicated in real-time fMRI-guided brain regulation and extend them by highlighting neuroanatomical topography relevant to self-regulation of emotion-related brain nodes. However, considering the small sample size any conclusion from the observed effects should be cautious. Further studies with larger samples, adopting homogenous experimental protocols, are still required. In particular, future studies should explore brain structural landmarks at both macro- and mesoscale specifically contributing to specific emotional brain regulation strategies in contrast to more general regulatory mechanisms. In the field of cognitive emotion regulation it has been proposed a distinction, with some overlaps, between brain circuits supporting emotion regulation and those contributing to general neurophysiological regulation (Gross 2014). An analogous perspective is plausible in the context of real-time fMRI-based emotional brain regulation. Ultimately, we reason that neuroanatomical predictors, along with other important methodological factors shown to impact real-time fMRI-based regulation (Haugg et al. 2021), might be relevant for designing and optimizing future protocols of patient-tailored interventions for emotional disorders.

Declarations

Acknowledgments

This research did not receive any specific grant from funding agencies in the public, commercial, or not-for-profit sectors.

Conflict of Interest

Authors have no financial and non-financial conflicts of interest to declare.

Author contributions

AC and AG conceived, designed research, analyzed data; AC drafted manuscript; AC and AG edited, revised and approved the final version of manuscript.

Data availability statement

The datasets generated during and/or analyzed during the current study are available from the corresponding author on reasonable request.

References

1. Ashburner J, Friston KJ (2005) Unified segmentation. Neuroimage 26 (3):839–851. doi:10.1016/j.neuroimage.2005.02.018
2. Baumann O, Mattingley JB (2012) Functional topography of primary emotion processing in the human cerebellum. Neuroimage 61 (4):805–811. doi:10.1016/j.neuroimage.2012.03.044
3. Berman BD, Horovitz SG, Hallett M (2013) Modulation of functionally localized right insular cortex activity using real-time fMRI-based neurofeedback. Front Hum Neurosci 7:638. doi:10.3389/fnhum.2013.00638
4. Bostan AC, Dum RP, Strick PL (2013) Cerebellar networks with the cerebral cortex and basal ganglia. Trends Cogn Sci 17 (5):241–254. doi:10.1016/j.tics.2013.03.003
5. Bostan AC, Strick PL (2018) The basal ganglia and the cerebellum: nodes in an integrated network. Nat Rev Neurosci 19 (6):338–350. doi:10.1038/s41583-018-0002-7
6. Bruhl AB, Scherpiet S, Sulzer J, Stampfli P, Seifritz E, Herwig U (2014) Real-time neurofeedback using functional MRI could improve down-regulation of amygdala activity during emotional stimulation: a proof-of-concept study. Brain topography 27 (1):138–148. doi:10.1007/s10548-013-0331-9
7. Buhle JT, Silvers JA, Wager TD, Lopez R, Onyemekwu C, Kober H, Weber J, Ochsner KN (2014) Cognitive reappraisal of emotion: a meta-analysis of human neuroimaging studies. Cereb Cortex 24 (11):2981–2990. doi:10.1093/cercor/bht154
8. Caballero-Gaudes C, Reynolds RC (2017) Methods for cleaning the BOLD fMRI signal. Neuroimage 154:128–149. doi:10.1016/j.neuroimage.2016.12.018
9. Caria A (2016) Self-Regulation of Blood Oxygenation Level Dependent Response: Primary Effect or Epiphenomenon? Front Neurosci 10:117. doi:10.3389/fnins.2016.00117
10. Caria A (2020) Mesocorticolimbic Interactions Mediate fMRI-Guided Regulation of Self-Generated Affective States. Brain Sci 10 (4). doi:10.3390/brainsci10040223
11. Caria A, Sitaram R, Birbaumer N (2012) Real-time fMRI: a tool for local brain regulation. Neuroscientist 18 (5):487–501. doi:10.1177/1073858411407205
12. Caria A, Sitaram R, Veit R, Begliomini C, Birbaumer N (2010) Volitional control of anterior insula activity modulates the response to aversive stimuli. A real-time functional magnetic resonance imaging study. Biol Psychiatry 68 (5):425–432. doi:10.1016/j.biopsych.2010.04.020 S0006-3223(10)00404-X [pii]
13. Caria A, Veit R, Sitaram R, Lotze M, Weiskopf N, Grodd W, Birbaumer N (2007) Regulation of anterior insular cortex activity using real-time fMRI. Neuroimage 35 (3):1238–1246. doi:S1053-8119(07)00038-9 [pii] 1016/j.neuroimage.2007.01.018
14. Cohen Kadosh K, Luo Q, de Burca C, Sokunbi MO, Feng J, Linden DEJ, Lau JYF (2016) Using real-time fMRI to influence effective connectivity in the developing emotion regulation network. Neuroimage 125:616–626. doi:10.1016/j.neuroimage.2015.09.070
15. Cremers HR, Wager TD, Yarkoni T (2017) The relation between statistical power and inference in fMRI. PLoS One 12 (11):e0184923. doi:10.1371/journal.pone.0184923
16. Damoiseaux JS, Rombouts SA, Barkhof F, Scheltens P, Stam CJ, Smith SM, Beckmann CF (2006) Consistent resting-state networks across healthy subjects. Proc Natl Acad Sci U S A 103 (37):13848–13853. doi:10.1073/pnas.0601417103
17. Dohmatob E, Dumas G, Bzdok D (2020) Dark control: The default mode network as a reinforcement learning agent. Hum Brain Mapp 41 (12):3318–3341. doi:10.1002/hbm.25019
18. Doucet GE, Lee WH, Frangou S (2019) Evaluation of the spatial variability in the major resting-state networks across human brain functional atlases. Hum Brain Mapp 40 (15):4577–4587. doi:10.1002/hbm.24722
19. Emmert K, Kopel R, Sulzer J, Bruhl AB, Berman BD, Linden DEJ, Horovitz SG, Breimhorst M, Caria A, Frank S, Johnston S, Long Z, Paret C, Robineau F, Veit R, Bartsch A, Beckmann CF, Van De Ville D, Haller S (2016) Meta-analysis of real-time fMRI neurofeedback studies

using individual participant data: How is brain regulation mediated? Neuroimage 124 (Pt A):806–812. doi:10.1016/j.neuroimage.2015.09.042

20. Etkin A, Buchel C, Gross JJ (2015) The neural bases of emotion regulation. Nat Rev Neurosci 16 (11):693–700. doi:10.1038/nrn4044
21. Galea JM, Vazquez A, Pasricha N, de Xivry JJ, Celnik P (2011) Dissociating the roles of the cerebellum and motor cortex during adaptive learning: the motor cortex retains what the cerebellum learns. Cereb Cortex 21 (8):1761–1770. doi:10.1093/cercor/bhq246
22. Gaume A, Vialatte A, Mora-Sanchez A, Ramdani C, Vialatte FB (2016) A psychoengineering paradigm for the neurocognitive mechanisms of biofeedback and neurofeedback. Neurosci Biobehav Rev 68:891–910. doi:10.1016/j.neubiorev.2016.06.012
23. Grecucci A, Giorgetta C, Bonini N, Sanfey AG (2013a) Reappraising social emotions: the role of inferior frontal gyrus, temporo-parietal junction and insula in interpersonal emotion regulation. Front Hum Neurosci 7:523. doi:10.3389/fnhum.2013.00523
24. Grecucci A, Giorgetta C, Van't Wout M, Bonini N, Sanfey AG (2013b) Reappraising the ultimatum: an fMRI study of emotion regulation and decision making. Cereb Cortex 23 (2):399–410. doi:10.1093/cercor/bhs028
25. Grone M, Dyck M, Koush Y, Bergert S, Mathiak KA, Alawi EM, Elliott M, Mathiak K (2015) Upregulation of the rostral anterior cingulate cortex can alter the perception of emotions: fMRI-based neurofeedback at 3 and 7 T. Brain topography 28 (2):197–207. doi:10.1007/s10548-014-0384-4
26. Gross JJ (2014) Handbook of Emotion Regulation. Guilford Publications, New York
27. Hamilton JP, Glover GH, Hsu JJ, Johnson RF, Gotlib IH (2011) Modulation of subgenual anterior cingulate cortex activity with real-time neurofeedback. Hum Brain Mapp 32 (1):22–31. doi:10.1002/hbm.20997
28. Haugg A, Renz FM, Nicholson AA, Lor C, Gotzendorfer SJ, Sladky R, Skouras S, McDonald A, Craddock C, Hellrung L, Kirschner M, Herdener M, Koush Y, Papoutsi M, Keynan J, Hendler T, Cohen Kadosh K, Zich C, Kohl SH, Hallschmid M, MacInnes J, Adcock RA, Dickerson KC, Chen NK, Young K, Bodurka J, Marxen M, Yao S, Becker B, Auer T, Schweizer R, Pamplona G, Lanius RA, Emmert K, Haller S, Van De Ville D, Kim DY, Lee JH, Marins T, Megumi F, Sorger B, Kamp T, Liew SL, Veit R, Spetter M, Weiskopf N, Scharnowski F, Steyrl D (2021) Predictors of real-time fMRI neurofeedback performance and improvement - A machine learning mega-analysis. Neuroimage 237:118207. doi:10.1016/j.neuroimage.2021.118207
29. Haugg A, Sladky R, Skouras S, McDonald A, Craddock C, Kirschner M, Herdener M, Koush Y, Papoutsi M, Keynan JN, Hendler T, Cohen Kadosh K, Zich C, MacInnes J, Adcock RA, Dickerson K, Chen NK, Young K, Bodurka J, Yao S, Becker B, Auer T, Schweizer R, Pamplona G, Emmert K, Haller S, Van De Ville D, Blefari ML, Kim DY, Lee JH, Marins T, Fukuda M, Sorger B, Kamp T, Liew SL, Veit R, Spetter M, Weiskopf N, Scharnowski F (2020) Can we predict real-time fMRI neurofeedback learning success from pretraining brain activity? Hum Brain Mapp 41 (14):3839–3854. doi:10.1002/hbm.25089
30. Heffley W, Hull C (2019) Classical conditioning drives learned reward prediction signals in climbing fibers across the lateral cerebellum. eLife 8. doi:10.7554/eLife.46764
31. Hellrung L, Dietrich A, Hollmann M, Pleger B, Kalberlah C, Roggenhofer E, Villringer A, Horstmann A (2018) Intermittent compared to continuous real-time fMRI neurofeedback boosts control over amygdala activation. Neuroimage 166:198–208. doi:10.1016/j.neuroimage.2017.10.031
32. Herwig U, Lutz J, Scherpiet S, Scheerer H, Kohlberg J, Opialla S, Preuss A, Steiger VR, Sulzer J, Weidt S, Stampfli P, Rufer M, Seifritz E, Jancke L, Bruhl AB (2019) Training emotion regulation through real-time fMRI neurofeedback of amygdala activity. Neuroimage 184:687–696. doi:10.1016/j.neuroimage.2018.09.068
33. Hua K, Zhang J, Wakana S, Jiang H, Li X, Reich DS, Calabresi PA, Pekar JJ, van Zijl PC, Mori S (2008) Tract probability maps in stereotaxic spaces: analyses of white matter anatomy and tract-specific quantification. Neuroimage 39 (1):336–347. doi:10.1016/j.neuroimage.2007.07.053
34. Ito M (2008) Control of mental activities by internal models in the cerebellum. Nat Rev Neurosci 9 (4):304–313. doi:10.1038/nrn2332
35. Kohn N, Eickhoff SB, Scheller M, Laird AR, Fox PT, Habel U (2014) Neural network of cognitive emotion regulation–an ALE meta-analysis and MACM analysis. Neuroimage 87:345–355. doi:10.1016/j.neuroimage.2013.11.001
36. Kong R, Li J, Orban C, Sabuncu MR, Liu H, Schaefer A, Sun N, Zuo XN, Holmes AJ, Eickhoff SB, Yeo BTT (2019) Spatial Topography of Individual-Specific Cortical Networks Predicts Human Cognition, Personality, and Emotion. Cereb Cortex 29 (6):2533–2551. doi:10.1093/cercor/bhy123
37. Kostadinov D, Beau M, Blanco-Pozo M, Hausser M (2019) Predictive and reactive reward signals conveyed by climbing fiber inputs to cerebellar Purkinje cells. Nat Neurosci 22 (6):950–962. doi:10.1038/s41593-019-0381-8
38. Koush Y, Meskaldji DE, Pichon S, Rey G, Rieger SW, Linden DE, Van De Ville D, Vuilleumier P, Scharnowski F (2017) Learning Control Over Emotion Networks Through Connectivity-Based Neurofeedback. Cereb Cortex 27 (2):1193–1202. doi:10.1093/cercor/bhv311

39. LaBar KS, Cabeza R (2006) Cognitive neuroscience of emotional memory. Nat Rev Neurosci 7 (1):54–64. doi:10.1038/nrn1825
40. Larry N, Yarkoni M, Lixenberg A, Joshua M (2019) Cerebellar climbing fibers encode expected reward size. eLife 8. doi:10.7554/eLife.46870
41. Lawrence EJ, Su L, Barker GJ, Medford N, Dalton J, Williams SC, Birbaumer N, Veit R, Ranganatha S, Bodurka J, Brammer M, Giampietro V, David AS (2013) Self-regulation of the anterior insula: Reinforcement learning using real-time fMRI neurofeedback. Neuroimage 88C:113–124. doi:10.1016/j.neuroimage.2013.10.069
42. Lee S, Ruiz S, Caria A, Veit R, Birbaumer N, Sitaram R (2011) Detection of cerebral reorganization induced by real-time fMRI feedback training of insula activation: a multivariate investigation. Neurorehabil Neural Repair 25 (3):259–267. doi:10.1177/1545968310385128
43. Linden DE, Habes I, Johnston SJ, Linden S, Tatineni R, Subramanian L, Sorger B, Healy D, Goebel R (2012) Real-time self-regulation of emotion networks in patients with depression. PLoS One 7 (6):e38115. doi:10.1371/journal.pone.0038115
44. Linhartova P, Latalova A, Kosa B, Kasparek T, Schmahl C, Paret C (2019) fMRI neurofeedback in emotion regulation: A literature review. Neuroimage 193:75–92. doi:10.1016/j.neuroimage.2019.03.011
45. Lubianiker N, Goldway N, Fruchtman-Steinbok T, Paret C, Keynan JN, Singer N, Cohen A, Kadosh KC, Linden DEJ, Hendler T (2019) Process-based framework for precise neuromodulation. Nat Hum Behav 3 (5):436–445. doi:10.1038/s41562-019-0573-y
46. Marxen M, Jacob MJ, Muller DK, Posse S, Ackley E, Hellrung L, Riedel P, Bender S, Epple R, Smolka MN (2016) Amygdala Regulation Following fMRI-Neurofeedback without Instructed Strategies. Front Hum Neurosci 10:183. doi:10.3389/fnhum.2016.00183
47. Mehler DMA, Sokunbi MO, Habes I, Barawi K, Subramanian L, Range M, Evans J, Hood K, Luhrs M, Keedwell P, Goebel R, Linden DEJ (2018) Targeting the affective brain-a randomized controlled trial of real-time fMRI neurofeedback in patients with depression. Neuropsychopharmacology: official publication of the American College of Neuropsychopharmacology 43 (13):2578–2585. doi:10.1038/s41386-018-0126-5
48. Messina I, Grecucci A, Viviani R (2021) Neurobiological models of emotion regulation: a meta-analysis of neuroimaging studies of acceptance as an emotion regulation strategy. Soc Cogn Affect Neurosci 16 (3):257–267. doi:10.1093/scan/nsab007
49. Misaki M, Phillips R, Zotev V, Wong CK, Wurfel BE, Krueger F, Feldner M, Bodurka J (2018) Real-time fMRI amygdala neurofeedback positive emotional training normalized resting-state functional connectivity in combat veterans with and without PTSD: a connectome-wide investigation. NeuroImage Clinical 20:543–555. doi:10.1016/j.nicl.2018.08.025
50. Morgenroth E, Saviola F, Gilleen J, Allen B, Luhrs M, M WE, Allen P (2020) Using connectivity-based real-time fMRI neurofeedback to modulate attentional and resting state networks in people with high trait anxiety. NeuroImage Clinical 25:102191. doi:10.1016/j.nicl.2020.102191
51. Mori S, Oishi K, Jiang H, Jiang L, Li X, Akhter K, Hua K, Faria AV, Mahmood A, Woods R, Toga AW, Pike GB, Neto PR, Evans A, Zhang J, Huang H, Miller MI, van Zijl P, Mazziotta J (2008) Stereotaxic white matter atlas based on diffusion tensor imaging in an ICBM template. Neuroimage 40 (2):570–582. doi:10.1016/j.neuroimage.2007.12.035
52. Ochsner KN, Silvers JA, Buhle JT (2012) Functional imaging studies of emotion regulation: a synthetic review and evolving model of the cognitive control of emotion. Ann N Y Acad Sci 1251:E1-24. doi:10.1111/j.1749-6632.2012.06751.x
53. Papageorgiou TD, Lisinski JM, McHenry MA, White JP, LaConte SM (2013) Brain-computer interfaces increase whole-brain signal to noise. Proc Natl Acad Sci U S A 110 (33):13630–13635. doi:10.1073/pnas.1210738110
54. Paret C, Goldway N, Zich C, Keynan JN, Hendler T, Linden D, Cohen Kadosh K (2019a) Current progress in real-time functional magnetic resonance-based neurofeedback: Methodological challenges and achievements. Neuroimage 202:116107. doi:10.1016/j.neuroimage.2019.116107
55. Paret C, Hendler T (2020) Live from the "regulating brain": Harnessing the brain to change emotion. Emotion 20 (1):126–131. doi:10.1037/emo0000674
56. Paret C, Kluetsch R, Ruf M, Demirakca T, Hoesterey S, Ende G, Schmahl C (2014) Down-regulation of amygdala activation with real-time fMRI neurofeedback in a healthy female sample. Front Behav Neurosci 8:299. doi:10.3389/fnbeh.2014.00299
57. Paret C, Kluetsch R, Zaehringer J, Ruf M, Demirakca T, Bohus M, Ende G, Schmahl C (2016a) Alterations of amygdala-prefrontal connectivity with real-time fMRI neurofeedback in BPD patients. Soc Cogn Affect Neurosci 11 (6):952–960. doi:10.1093/scan/nsw016
58. Paret C, Ruf M, Gerchen MF, Kluetsch R, Demirakca T, Jungkunz M, Bertsch K, Schmahl C, Ende G (2016b) fMRI neurofeedback of amygdala response to aversive stimuli enhances prefrontal-limbic brain connectivity. Neuroimage 125:182–188. doi:10.1016/j.neuroimage.2015.10.027

59. Paret C, Zaehringer J, Ruf M, Ende G, Schmahl C (2019b) The orbitofrontal cortex processes neurofeedback failure signals. Behav Brain Res 369:111938. doi:10.1016/j.bbr.2019.111938
60. Paret C, Zahringer J, Ruf M, Gerchen MF, Mall S, Hendler T, Schmahl C, Ende G (2018) Monitoring and control of amygdala neurofeedback involves distributed information processing in the human brain. Hum Brain Mapp. doi:10.1002/hbm.24057
61. Pierce JE, Peron J (2020) The basal ganglia and the cerebellum in human emotion. Soc Cogn Affect Neurosci 15 (5):599–613. doi:10.1093/scan/nsaa076
62. Poldrack RA (2007) Region of interest analysis for fMRI. Soc Cogn Affect Neurosci 2 (1):67–70. doi:10.1093/scan/nsm006
63. Ramot M, Grossman S, Friedman D, Malach R (2016) Covert neurofeedback without awareness shapes cortical network spontaneous connectivity. Proc Natl Acad Sci U S A 113 (17):E2413-2420. doi:10.1073/pnas.1516857113
64. Ramot M, Kimmich S, Gonzalez-Castillo J, Roopchansingh V, Popal H, White E, Gotts SJ, Martin A (2017) Direct modulation of aberrant brain network connectivity through real-time NeuroFeedback. eLife 6. doi:10.7554/eLife.28974
65. Ritchey M, Wang SF, Yonelinas AP, Ranganath C (2019) Dissociable medial temporal pathways for encoding emotional item and context information. Neuropsychologia 124:66–78. doi:10.1016/j.neuropsychologia.2018.12.015
66. Ruiz S, Lee S, Soekadar SR, Caria A, Veit R, Kircher T, Birbaumer N, Sitaram R (2013) Acquired self-control of insula cortex modulates emotion recognition and brain network connectivity in schizophrenia. Hum Brain Mapp 34 (1):200–212. doi:10.1002/hbm.21427
67. Scheinost D, Stoica T, Saksa J, Papademetris X, Constable RT, Pittenger C, Hampson M (2013) Orbitofrontal cortex neurofeedback produces lasting changes in contamination anxiety and resting-state connectivity. Translational psychiatry 3:e250. doi:10.1038/tp.2013.24
68. Schrouff J, Monteiro JM, Portugal L, Rosa MJ, Phillips C, Mourao-Miranda J (2018) Embedding Anatomical or Functional Knowledge in Whole-Brain Multiple Kernel Learning Models. Neuroinformatics 16 (1):117–143. doi:10.1007/s12021-017-9347-8
69. Schrouff J, Rosa MJ, Rondina JM, Marquand AF, Chu C, Ashburner J, Phillips C, Richiardi J, Mourao-Miranda J (2013) PRoNTo: pattern recognition for neuroimaging toolbox. Neuroinformatics 11 (3):319–337. doi:10.1007/s12021-013-9178-1
70. Schutter DJ, van Honk J (2009) The cerebellum in emotion regulation: a repetitive transcranial magnetic stimulation study. Cerebellum 8 (1):28–34. doi:10.1007/s12311-008-0056-6
71. Sendhilnathan N, Semework M, Goldberg ME, Ipata AE (2020) Neural Correlates of Reinforcement Learning in Mid-lateral Cerebellum. Neuron 106 (1):188–198 e185. doi:10.1016/j.neuron.2019.12.032
72. Shibata K, Lisi G, Cortese A, Watanabe T, Sasaki Y, Kawato M (2019) Toward a comprehensive understanding of the neural mechanisms of decoded neurofeedback. Neuroimage 188:539–556. doi:10.1016/j.neuroimage.2018.12.022
73. Shibata K, Watanabe T, Kawato M, Sasaki Y (2016) Differential Activation Patterns in the Same Brain Region Led to Opposite Emotional States. PLoS Biol 14 (9):e1002546. doi:10.1371/journal.pbio.1002546
74. Sitaram R, Caria A, Veit R, Gaber T, Ruiz S, Birbaumer N (2014) Volitional control of the anterior insula in criminal psychopaths using real-time fMRI neurofeedback: A pilot study. Frontiers in Behavioral Neuroscience:In press
75. Sitaram R, Ros T, Stoeckel L, Haller S, Scharnowski F, Lewis-Peacock J, Weiskopf N, Blefari ML, Rana M, Oblak E, Birbaumer N, Sulzer J (2017) Closed-loop brain training: the science of neurofeedback. Nat Rev Neurosci 18 (2):86–100. doi:10.1038/nrn.2016.164
76. Skottnik L, Sorger B, Kamp T, Linden D, Goebel R (2019) Success and failure of controlling the real-time functional magnetic resonance imaging neurofeedback signal are reflected in the striatum. Brain Behav 9 (3):e01240. doi:10.1002/brb3.1240
77. Smith SM, Fox PT, Miller KL, Glahn DC, Fox PM, Mackay CE, Filippini N, Watkins KE, Toro R, Laird AR, Beckmann CF (2009) Correspondence of the brain's functional architecture during activation and rest. Proc Natl Acad Sci U S A 106 (31):13040–13045. doi:10.1073/pnas.0905267106
78. Sokolov AA, Miall RC, Ivry RB (2017) The Cerebellum: Adaptive Prediction for Movement and Cognition. Trends Cogn Sci 21 (5):313–332. doi:10.1016/j.tics.2017.02.005
79. Spisak T, Spisak Z, Zunhammer M, Bingel U, Smith S, Nichols T, Kincses T (2018) Probabilistic TFCE: A generalized combination of cluster size and voxel intensity to increase statistical power. Neuroimage 185:12–26. doi:10.1016/j.neuroimage.2018.09.078
80. Spreng RN, Grady CL (2010) Patterns of brain activity supporting autobiographical memory, prospection, and theory of mind, and their relationship to the default mode network. J Cogn Neurosci 22 (6):1112–1123. doi:10.1162/jocn.2009.21282
81. Stelzer J, Lohmann G, Mueller K, Buschmann T, Turner R (2014) Deficient approaches to human neuroimaging. Front Hum Neurosci 8:462. doi:10.3389/fnhum.2014.00462
82. Suddendorf T, Corballis MC (2007) The evolution of foresight: What is mental time travel, and is it unique to humans? Behav Brain Sci 30 (3):299–313; discussion 313 – 251. doi:10.1017/S0140525X07001975

83. Sulzer J, Sitaram R, Blefari ML, Kollias S, Birbaumer N, Stephan KE, Luft A, Gassert R (2013) Neurofeedback-mediated self-regulation of the dopaminergic midbrain. Neuroimage 75C:176–184. doi:10.1016/j.neuroimage.2013.02.041
84. Swain RA, Kerr AL, Thompson RF (2011) The cerebellum: a neural system for the study of reinforcement learning. Front Behav Neurosci 5:8. doi:10.3389/fnbeh.2011.00008
85. Taschereau-Dumouchel V, Cortese A, Chiba T, Knotts JD, Kawato M, Lau H (2018) Towards an unconscious neural reinforcement intervention for common fears. Proc Natl Acad Sci U S A 115 (13):3470–3475. doi:10.1073/pnas.1721572115
86. Thibault RT, MacPherson A, Lifshitz M, Roth RR, Raz A (2018) Neurofeedback with fMRI: A critical systematic review. Neuroimage 172:786–807. doi:10.1016/j.neuroimage.2017.12.071
87. Togo H, Rokicki J, Yoshinaga K, Hisatsune T, Matsuda H, Haga N, Hanakawa T (2017) Effects of Field-Map Distortion Correction on Resting State Functional Connectivity MRI. Front Neurosci 11:656. doi:10.3389/fnins.2017.00656
88. Tzourio-Mazoyer N, Landeau B, Papathanassiou D, Crivello F, Etard O, Delcroix N, Mazoyer B, Joliot M (2002) Automated anatomical labeling of activations in SPM using a macroscopic anatomical parcellation of the MNI MRI single-subject brain. Neuroimage 15 (1):273–289. doi:10.1006/nimg.2001.0978
89. Van Overwalle F, Baetens K, Marien P, Vandekerckhove M (2014) Social cognition and the cerebellum: a meta-analysis of over 350 fMRI studies. Neuroimage 86:554–572. doi:10.1016/j.neuroimage.2013.09.033
90. Veit R, Singh V, Sitaram R, Caria A, Rauss K, Birbaumer N (2012) Using real-time fMRI to learn voluntary regulation of the anterior insula in the presence of threat-related stimuli. Soc Cogn Affect Neurosci 7 (6):623–634. doi:10.1093/scan/nsr061
91. Wagner MJ, Kim TH, Savall J, Schnitzer MJ, Luo L (2017) Cerebellar granule cells encode the expectation of reward. Nature 544 (7648):96–100. doi:10.1038/nature21726
92. Watanabe T, Sasaki Y, Shibata K, Kawato M (2017) Advances in fMRI Real-Time Neurofeedback. Trends Cogn Sci 21 (12):997–1010. doi:10.1016/j.tics.2017.09.010
93. Worsley KJ, Friston KJ (1995) Analysis of fMRI time-series revisited–again. Neuroimage 2 (3):173–181. doi:10.1006/nimg.1995.1023
94. Yang D, Pelphrey KA, Sukhodolsky DG, Crowley MJ, Dayan E, Dvornek NC, Venkataraman A, Duncan J, Staib L, Ventola P (2016) Brain responses to biological motion predict treatment outcome in young children with autism. Translational psychiatry 6 (11):e948. doi:10.1038/tp.2016.213
95. Yao S, Becker B, Geng Y, Zhao Z, Xu X, Zhao W, Ren P, Kendrick KM (2016) Voluntary control of anterior insula and its functional connections is feedback-independent and increases pain empathy. Neuroimage 130:230–240. doi:10.1016/j.neuroimage.2016.02.035
96. Young KD, Misaki M, Harmer CJ, Victor T, Zotev V, Phillips R, Siegle GJ, Drevets WC, Bodurka J (2017a) Real-Time Functional Magnetic Resonance Imaging Amygdala Neurofeedback Changes Positive Information Processing in Major Depressive Disorder. Biol Psychiatry 82 (8):578–586. doi:10.1016/j.biopsych.2017.03.013
97. Young KD, Siegle GJ, Misaki M, Zotev V, Phillips R, Drevets WC, Bodurka J (2018a) Altered task-based and resting-state amygdala functional connectivity following real-time fMRI amygdala neurofeedback training in major depressive disorder. NeuroImage Clinical 17:691–703. doi:10.1016/j.nicl.2017.12.004
98. Young KD, Siegle GJ, Zotev V, Phillips R, Misaki M, Yuan H, Drevets WC, Bodurka J (2017b) Randomized Clinical Trial of Real-Time fMRI Amygdala Neurofeedback for Major Depressive Disorder: Effects on Symptoms and Autobiographical Memory Recall. Am J Psychiatry 174 (8):748–755. doi:10.1176/appi.ajp.2017.16060637
99. Young KD, Zotev V, Phillips R, Misaki M, Drevets WC, Bodurka J (2018b) Amygdala real-time functional magnetic resonance imaging neurofeedback for major depressive disorder: A review. Psychiatry Clin Neurosci 72 (7):466–481. doi:10.1111/pcn.12665
100. Yuan H, Young KD, Phillips R, Zotev V, Misaki M, Bodurka J (2014) Resting-state functional connectivity modulation and sustained changes after real-time functional magnetic resonance imaging neurofeedback training in depression. Brain connectivity 4 (9):690–701. doi:10.1089/brain.2014.0262
101. Zhao Z, Yao S, Zweerings J, Zhou X, Zhou F, Kendrick KM, Chen H, Mathiak K, Becker B (2021) Putamen volume predicts real-time fMRI neurofeedback learning success across paradigms and neurofeedback target regions. Hum Brain Mapp 42 (6):1879–1887. doi:10.1002/hbm.25336
102. Zilverstand A, Sorger B, Sarkheil P, Goebel R (2015) fMRI neurofeedback facilitates anxiety regulation in females with spider phobia. Front Behav Neurosci 9:148. doi:10.3389/fnbeh.2015.00148
103. Zotev V, Krueger F, Phillips R, Alvarez RP, Simmons WK, Bellgowan P, Drevets WC, Bodurka J (2011) Self-regulation of amygdala activation using real-time FMRI neurofeedback. PLoS One 6 (9):e24522. doi:10.1371/journal.pone.0024522 PONE-D-11-06642 [pii]

104. Zotev V, Phillips R, Misaki M, Wong CK, Wurfel BE, Krueger F, Feldner M, Bodurka J (2018) Real-time fMRI neurofeedback training of the amygdala activity with simultaneous EEG in veterans with combat-related PTSD. NeuroImage Clinical 19:106–121. doi:10.1016/j.nicl.2018.04.010

105. Zotev V, Yuan H, Misaki M, Phillips R, Young KD, Feldner MT, Bodurka J (2016) Correlation between amygdala BOLD activity and frontal EEG asymmetry during real-time fMRI neurofeedback training in patients with depression. NeuroImage Clinical 11:224–238. doi:10.1016/j.nicl.2016.02.003

106. Zweerings J, Pflieger EM, Mathiak KA, Zvyagintsev M, Kacela A, Flatten G, Mathiak K (2018) Impaired Voluntary Control in PTSD: Probing Self-Regulation of the ACC With Real-Time fMRI. Front Psychiatry 9:219. doi:10.3389/fpsyt.2018.00219

Figures

Figure 1

% BOLD signal changes during AI regulation

Violin plots represent % BOLD signal change in the AI during real-time fMRI-guided regulation runs. White circles show the medians; box limits indicate the 25th and 75th percentiles as determined by the R software; whiskers extend 1.5 times the interquartile range from the 25th and 75th percentiles; polygons represent density estimates of % BOLD values and extend to extreme values. Violin plots were created with BoxPLotR (http://shiny.chemgrid.org/boxplotr).

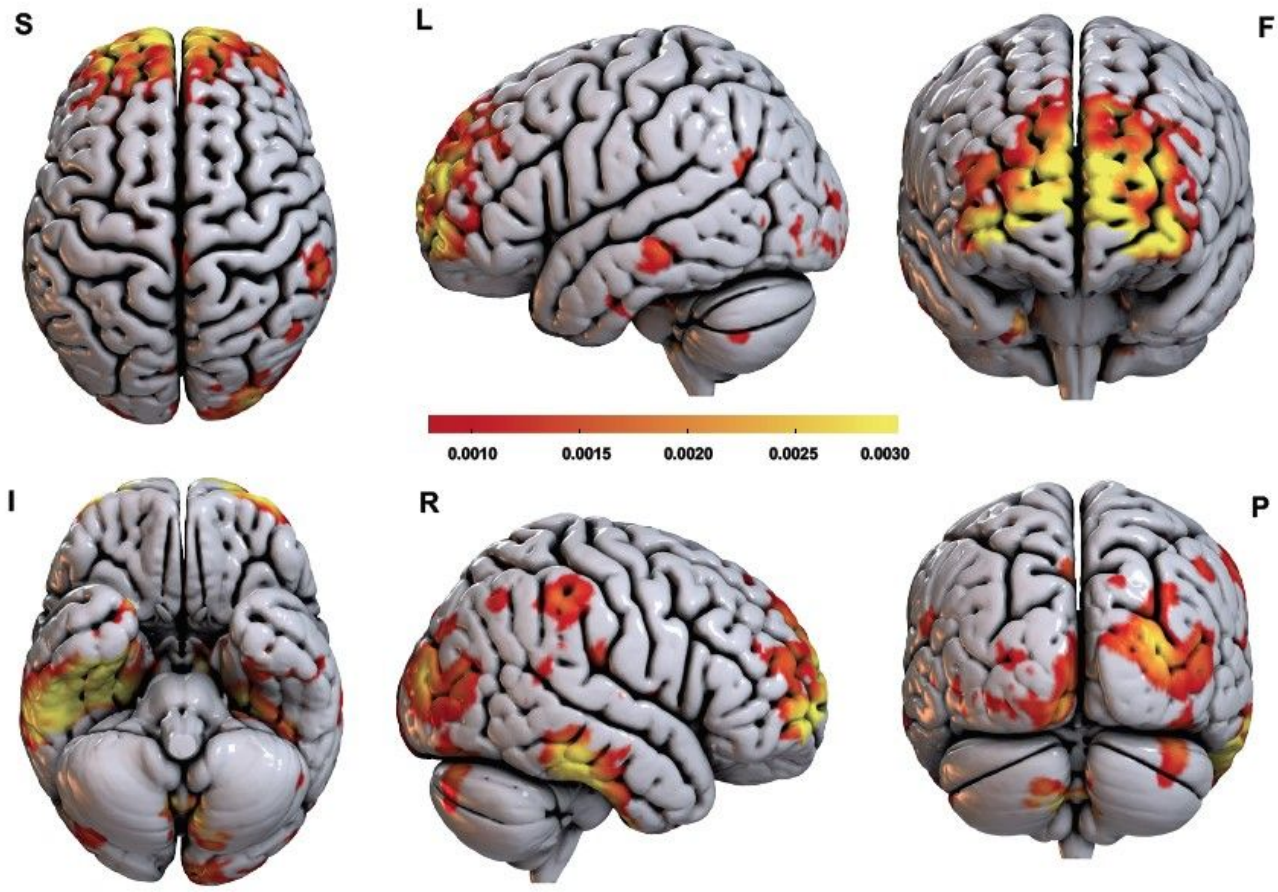

Figure 2

GM regions predictive of AI regulation

Whole brain images of GM weights map of KRR model indicating voxel-based contribution to explain averaged AI activity during all regulation runs. The colour bar refers to the weight of each voxel for decoding % BOLD signal change in the AI. Voxel-based predictive values were used to compute the total normalized weight of each anatomically labelled GM region, as reported in Table 1.

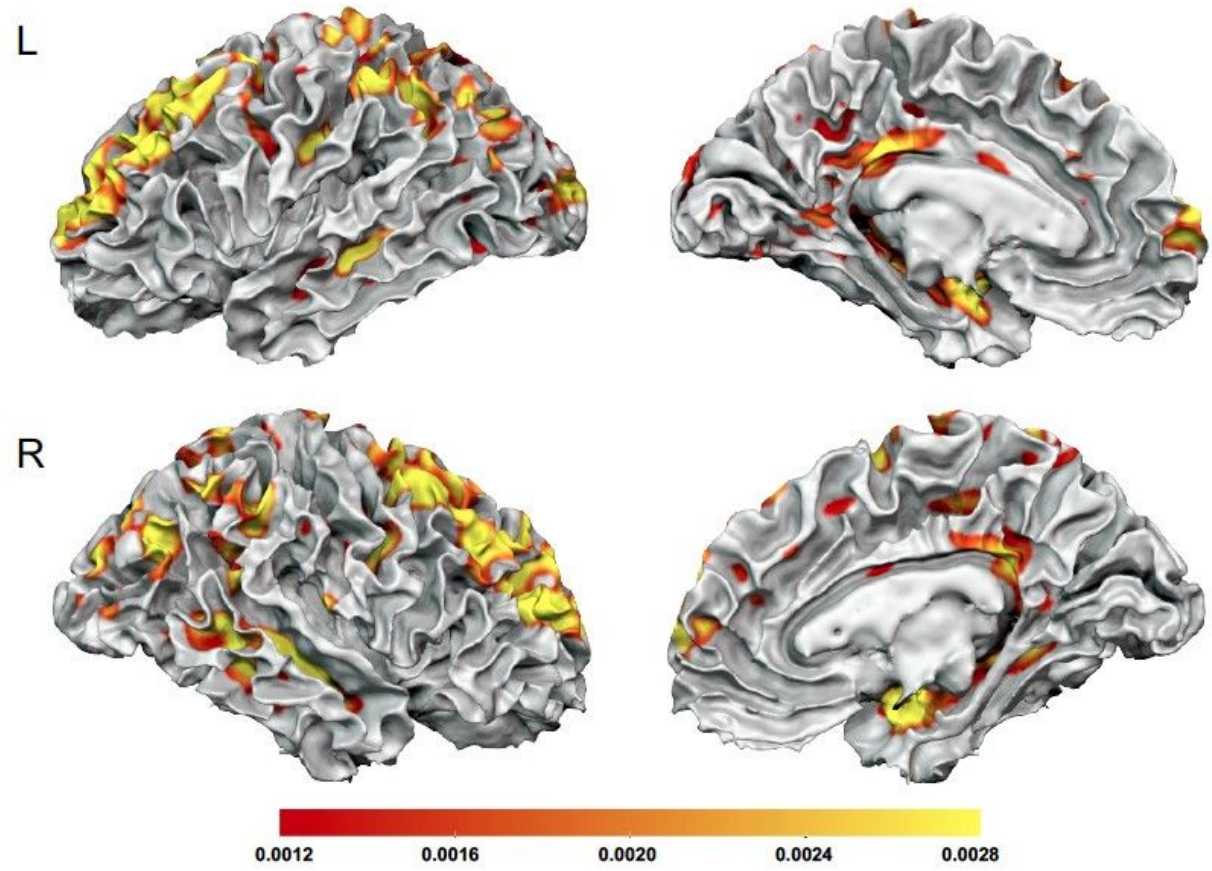

Figure 3

WM regions predictive of AI regulation

Whole brain images of WM weights map of KRR model indicating voxel-based contribution to explain averaged AI activity during all regulation runs. The colour bar refers to the weight of each voxel for decoding % BOLD signal change in the AI. Voxel-based predictive values were used to compute the total normalized weight of each anatomically labelled WM region, as reported in Table 3.